Charged carrier spin dynamics in ZnO quantum wells and epilayers

Jungtaek Kim, J. Puls,* S. Sadofev, and F. Henneberger†
AG Photonik, Institut für Physik, Humboldt-Universität zu Berlin, Newtonstr. 15, D-12489 Berlin, Germany
(Received 4 August 2015; revised manuscript received 21 December 2015; published 14 January 2016)

Longitudinal charged carrier spin dynamics is studied for ZnO quantum wells and epilayers using the optical transition of the negatively charged exciton X^- and the neutral donor bound exciton D^0X, respectively. The hole spin relaxation is derived from the optical orientation of X^- and D^0X photoluminescence, whereas the spin relaxation of the resident electrons and donor electrons is accessed via the bleaching of the spin selective excitation process. Hole spin relaxation times of $\tau_1^{s,h}$ of 80 and 140 ps are found for D^0X and X^-, respectively, which are practically independent of a magnetic field $B_\parallel$ applied along the ZnO $\vec{c}$ axis. Much longer longitudinal electron spin relaxation times in the 1 μs range are uncovered if the hyperfine interaction is suppressed by a proper $B_\parallel$. A field strength of $\approx$2 mT is large enough proving the extremely small value of the Overhauser field in ZnO. This is related to the very restricted number of magnetic nuclei interacting with the electron inside the volume of the exciton complex.

DOI: 10.1103/PhysRevB.93.045306

I. INTRODUCTION

ZnO and related heterostructures with a wide band gap have attracted large interest for transparent electronics and optoelectronics in the ultraviolet range [1]. Moreover, ZnO is considered as a potential material for spintronic applications. For electrons, the Elliot-Yafet spin relaxation mechanism scales with the squared ratio between hole spin-orbit (SO) coupling and the gap energy, yielding a dramatic reduction of this mechanism in bulk ZnO compared to, e.g., GaAs. Only the D'yakonov-Perel mechanism is expected to contribute significantly both in bulk and quantum well structures [2,3]. For localized electrons, the interaction with magnetic nuclei has to be additionally considered [2]. Despite the high interest on ZnO, optical studies on carrier spin dynamics are rather limited so far to bulk and epilayer samples. Ghosh *et al.* [3] studied the electron spin coherence in the conduction band by optically detected spin precession, yielding a $\tau_2^{s,e}$ time in the 10 ns range at low temperatures. Hole spin relaxation has been studied for the donor bound exciton D^0X using time-resolved optical orientation [4], spin precession [5], and time-resolved increase of polarization degree in a finite $B_\parallel$ after unpolarized, nonresonant excitation [6]. The recent proof of the negatively charged exciton X^- transitions in ZnO/(Zn,Mg)O quantum wells (QWs) [7] has offered a tool to trace carrier spin dynamics for ZnO in the case of reduced dimensionality, where usually an increased transversal and longitudinal spin relaxation time is expected [2].

In this paper, an exemplary study on the longitudinal carrier spin dynamic in ZnO related structures will be presented both for QWs and epitaxial layers grown under comparable conditions. The possibility of a reduced SO coupling via increased subvalence band splitting in ZnO QWs by strain and/or confinement as well as the role of hyperfine interaction (HFI) in ZnO with extremely diluted magnetic nuclei will be treated. Since X^- and D^0X in QWs and epilayers, respectively, possess the same spin configuration with paired electron spins, the hole spin can be directly traced by the circular polarized luminescence of both complexes. The spin dynamic of the resident QW and the donor electron is accessible via the bleaching of the initial state of the X^- and D^0X, respectively, photo-excitation [8]. The experiments are carried out using a static magnetic field $B_\parallel$ applied along the ZnO $\vec{c}$ axis parallel to the growth axis in the case of QWs.

II. EXPERIMENTAL

The samples are grown on a *c*-plane sapphire substrate by radical-source molecular beam epitaxy. First, a 2 nm MgO buffer layer is deposited at 650 °C and a 45 nm (Zn,Mg)O nucleation layer is grown at 360 °C followed by an annealing step at 730 °C. The subsequent 600 nm (Zn,Mg)O buffer layer is again grown at 360 °C and annealed at 680 °C. The active multiple QW (MQW) part consists of ten well-barrier combinations with widths of $d_w = 3.5$ and $d_b = 11$ nm, respectively, grown on this composite buffer. The Mg content in the buffer and the barriers amounts to $x_{Mg} = 0.09$. For the epilayer structure, the MQW range is replaced by a 140 nm ZnO layer and a 100 nm (Zn,Mg)O cap. Finally, an annealing step at 680 °C is applied to the complete structures. The use of this growth receipt provides high-quality ZnO/(Zn,Mg)O structures with atomically flat interfaces [9]. Excitation of time-integrated and time-resolved photoluminescence (PL) with tunable photon energy is performed by the frequency-doubled output of a mode-locked Pyridine 2 dye laser synchronously pumped by the second harmonic of a mode-locked Nd:YVO_4 laser. A three-plate birefringent filter is installed in the dye laser to reduce the spectral width of the frequency-doubled laser radiation to below 1 meV. Time-integrated PL and transmission spectra are taken by a spectrometer with a linear dispersion of 0.5 nm/mm and a liquid-nitrogen cooled CCD detector. Linear polarizers and $\lambda/4$ retardation plates are used in the excitation and detection path to control the respective light polarization. Spectrally resolved PL transients of both helicities are taken with an overall spectral and temporal resolution of 1.5 meV and 10 ps, respectively. After pulsed, circularly polarized excitation, the PL is spectrally dispersed by a double monochromator

*puls@physik.hu-berlin.de
†Deceased February 2015.

in subtractive mode and recorded by a streak camera in synchroscan mode. The hole spin dynamic is seen in the temporal development of the circular polarization degree $\rho(t) = [I_{\sigma^+}(t) - I_{\sigma^-}(t)]/[I_{\sigma^+}(t) + I_{\sigma^-}(t)]$ where $I_{\sigma^{+(-)}}(t)$ is the PL intensity for $\sigma^{+(-)}$ polarization. For studying the spin dynamic of resident electrons by saturation spectroscopy, a combination of a Pockels cell and $\lambda/4$ retardation plate in the excitation path is used to provide an alternating excitation of opposite helicity. The time-resolved PL is again dispersed by the double monochromator and recorded by a combination of microchannel-plate photomultiplier, preamplifier, and multi-scaler with overall 1 ns time resolution. The magnetic field is supplied by an Oxford split-coil magnet capable of fields up to $B = 12$ T. The samples are immersed in pumped liquid helium at a bath temperature of $T_b = 1.6$ K.

III. RESULTS AND DISCUSSION

In Figs. 1(a) and 1(b), PL and absorption spectra in the spectral vicinity of the A and B excitons [10] are summarized for the studied MQW and epilayer sample, where the indexes A and B denote the uppermost and next lower hole state, respectively. Below the free exciton absorption X_A and X_B in Fig. 1(a), a clearly resolved shoulder marks the charged exciton absorption X_A^- [7]. The pronounced PL band with a full width at half maximum (FWHM) of 7 meV is Stokes-shifted by ≈5 meV with respect to the absorption as typical feature of QW exciton complex localized by in-plane potential fluctuations. The D^0X_A PL and absorption in Fig. 1(b) have, as expected, clearly smaller half width and practically no Stokes shift. The correspondingly less pronounced low-energy wing of the free exciton absorption for the epilayer offers the possibility to detect the absorption of the D^0X_B at about a 5 meV higher photon energy. The very smooth surfaces of the epitaxially grown layers and the polished rear side of the substrate ensures an extremely low level of scattered laser light. Combined with a high quantum efficiency of the structures, this yields a ratio of more than 1:10 between the PL signal and the, mostly Rayleigh, scattered excitation light in the case of an

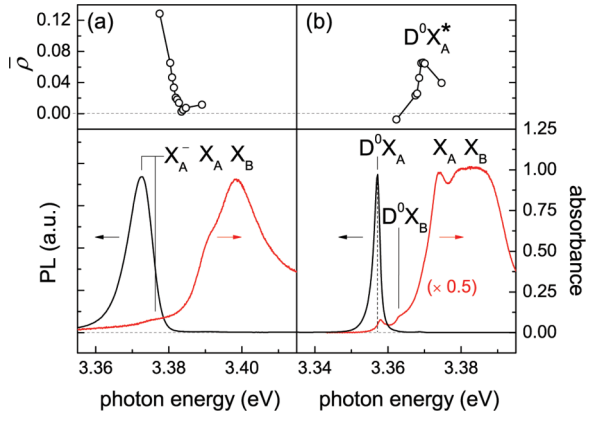

FIG. 1. PL (solid black lines) and absorption (solid red lines) spectra scaled at the left and right hand axis, respectively, of the (a) MQW and (b) epilayer sample. Upper panels: PL polarization degree $\overline{\rho}$ derived from the time-integrated spectra at selected excitation photon energies.

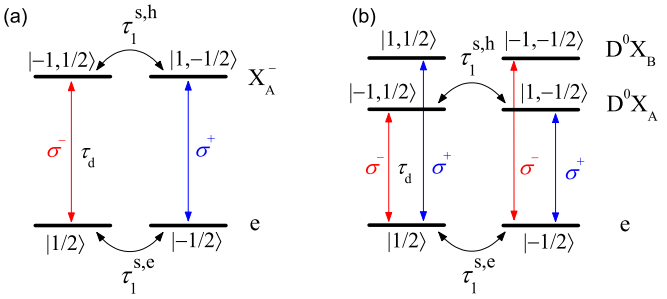

FIG. 2. Scheme of (a) X^- transition and (b) D^0X transition. The blue and red arrows indicate σ^+ and σ^-, respectively, circularly polarized excitation and recombination. $\tau_1^{s,e}$ ($\tau_1^{s,h}$) denotes the longitudinal electron (hole) spin relaxation time, τ_d the recombination time constant. The hole states in the X^- and D^0X complexes are denoted by $|\, m_l, m_s >$.

absorption of 0.1 and the same helicity of excitation and detection. For opposite helicity, the scattered light intensity drops and the ratio increases to 1:1. These facts allows us to detect a few meV energetically below excitation without any distortion from scattered excitation light. That means that for the charged exciton X_A^- a direct excitation in the Stokes shifted absorption and for donor bound exciton an excitation via the D^0X_B could be realized in the studies of the carrier spin dynamic.

In the upper panels of Fig. 1, the polarization degree $\overline{\rho}$ derived from the time-integrated PL is drawn around the interesting regions of excitation. A value of $\overline{\rho} \approx 0.1$ is found for X_A^- for excitation in its absorption maximum with a tendency to increase under excitation of more localized states at lower photon energy. Excitation of donor bound excitons via D^0X_B yields a negative $\overline{\rho}$ with somewhat smaller modulus and an increase to larger positive values with a maximum around 5 meV below the energy of X_A. Prior to a discussion of that feature, the excitation/detection scheme will be considered for X^- and D^0X in Figs. 2(a) and 2(b), respectively. Here, the widely accepted situation with Γ_7 symmetry of the uppermost A valence band [1,10,11] is considered which has been proven recently to be valid also in the case of ZnO QWs [7]. The positive $\overline{\rho}$ of X^- is a simple consequence of the direct excitation of the X^- complex involving a hole from the A valence band. The conversion of the excited D^0X_B to the D^0X_A bound exciton ground state, on the other hand, is expected to be surely more probable via changing the orbital quantum number m_l [vertical transition between the upper states in Fig. 2(b)] by the accompanied phonon emission than via a changing of m_s via a spin flip which explains the observed negative $\overline{\rho}$. The above mentioned excitation resonance about 11 meV above the D^0X_A ground state with positive $\overline{\rho}$ has been attributed to an excited D^0X_A state ($D^0X_A^*$) and used to study the hole spin memory in ZnO epilayer [4]. From the energetic position, a similarity with one of several excited D^0X state in CdS [12] can be stated where the hole moves around the donor core and the two electrons on a orbital with *d*-like symmetry. Such state gains a remarkable oscillator strength due to the coupling with the *s*-like hole orbital in the ground state via the *sd* coupling present in uniaxial crystals in effective mass approximation. We prefer here to carry out the studies

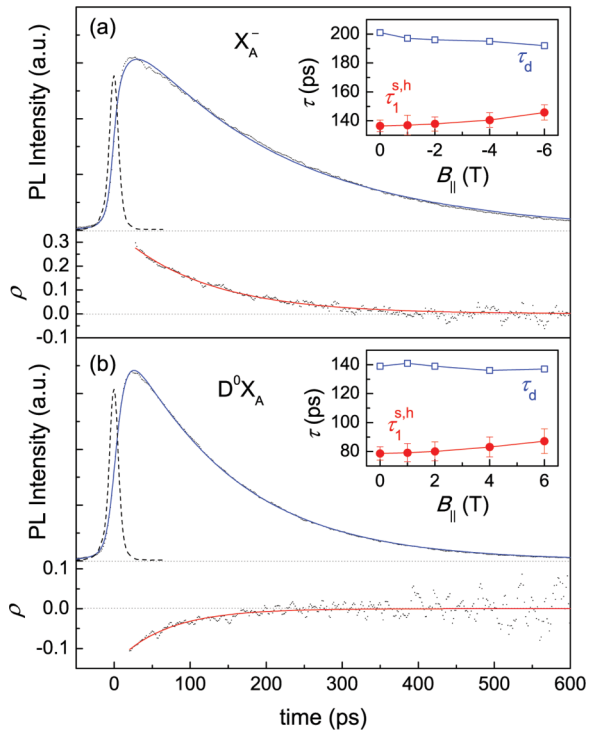

FIG. 3. Dots show the time-resolved PL intensity (upper panels) and circular polarization degree (lower panels) for the (a) X_A^- transition in the MQW and (b) D^0X transition in the epilayer sample. The solid (blue) lines in the upper panels are the deconvolution fit of the PL decay using the system response given by dashed curves (see text). The solid (red) lines in the lower panels represent the single-exponential fit of the $\rho(t)$ data. Insets: $B_\parallel$ dependence of the recombination time τ_d and the hole spin life time $\tau_1^{s,h}$.

on D^0X via the excitation of D^0X_B since an accompanied excitation of free excitons in the case of $D^0X_A^*$ is avoided and the condition of an absorption much smaller than unity, necessary for the saturation spectroscopy, is fulfilled. For X^-, the excitation is always at the X_A^- absorption peak in the following.

Before the hole spin relaxation data will be presented, the lifetime of the exciton complexes X_A^- and D^0X_A will be briefly considered. The respective decay transients are simply obtained by the sum of the measured PL transients $I(t) = I_{\sigma^+}(t) + I_{\sigma^-}(t)$ given by dots in the upper panels of Figs. 3(a) and 3(b) for X_A^- and D^0X_A, respectively, for $B_\parallel = 0$. Rise and decay times are extracted by a deconvolution using a response function $R(t) = -a_r \exp(-t/\tau_r) + a_d \exp(-t/\tau_d)$ and the system response given by dashed lines in the respective panels.

From the fit drawn by solid blue lines, X_A^- and D^0X_A lifetimes $\tau_d = 200$ and 140 ps, respectively, are obtained. Whereas such times are in the expected range for the lifetime of exciton complexes in ZnO QWs and bulk, it should be noted that non-single-exponential D^0X PL decays with time constants ranging from 200 ps to more than 1 ns are reported for bulk samples, i.e., commercially available ZnO substrates, with a variety of chemically different donors [13]. For ZnO epilayers grown on sapphire, lifetimes in the 100 to 160 ps range [4,14] are found in accord with the present result. The reason for such different PL decay constants are presently not clear. The deduced rise times τ_r in the order of 10 ps represent a measure for the localization time and B to A hole conversion rate of X_A^- and D^0X, respectively. It is emphasized that the lifetimes of the exciton complexes are practically independent of an applied $B_\parallel \leqslant 6$ T (see upper curve in the insets of Fig. 3) as expected in the studied field strength range due to the negligible diamagnetic interaction with the exciton complexes in ZnO tightly bound by Coulomb interaction [10].

The time-resolved optical orientation is plotted in the lower panels of Figs. 3(a) and 3(b) for X_A^- and D^0X_A, respectively. A single exponential decay of $\rho(t) \sim \exp(-t/\tau_1^{s,h})$ is used to fit the data and to extract the hole spin relaxation times. To avoid complications, the fit is restricted to times $t > 20$ ps where the spin pumping is finished. The longitudinal hole spin relaxation time of the D^0X_A $\tau_1^{s,h} = 80$ ps is in a reasonable agreement with the previously published data [4,6]. The values of $\tau_1^{s,h}$ are up to two orders of magnitude larger than those seen for free holes in the valence band of bulk GaAs [2,15,16]. Although a direct comparison of free and bound hole states is not straightforward, the distinctly larger hole spin relaxation time in bulk ZnO is surely related to its valence-band structure [10]. The upper A valence band with Γ_7 symmetry is a rather pure spin state due to the combined action of the crystal field and the much smaller SO interaction. The resulting mutual admixture of A and C bands with oppositely aligned spin amounts to only 1–2% and the hexagonal crystal structure leads to a finite splitting between the A and B bands already in the bulk case. These circumstances explain that the extremely small SO interaction not only favors an increased electron spin coherence as discussed in the Introduction, but also pushes $\tau_1^{s,h}$ into the 100 ps range for bulk ZnO. The longitudinal hole spin relaxation time found for the charged exciton in the QW $\tau_1^{s,h} = 140$ ps is only marginally larger than the bulk value. This seems not to be surprising since the conditions favorable for the hole spin are already present in the bulk case. Furthermore, the quantum confinement of the holes in ZnO QWs do only marginally vary the A-B valence band splitting since the rather congeneric orbital symmetry of Γ_7 and Γ_9 holes [10] with $m_l = \pm 1$ leads to practically the same strain-induced shift of both valence bands and provides similar hole masses in direction of the $\vec{c}$ axis and therefore similar confinement energies in present QW structures. One can speculate that weak coupling between A and C valence bands determines a rather fixed hole spin lifetime in the case of ZnO in obvious contrast to the *usual* semiconductors, where the hole spin relaxation is determined by the D'yakonov-Perel mechanism between the pure spin heavy-hole band and the light-hole band with a 1:2 admixture of spin up and spin down. If QWs are formed from zinc-blende compound semiconductors, the lifted degeneracy of heavy- and light-hole bands in the zone center can result indeed in a higher hole spin coherence [17,18]. To get finally an impression on the rigidity of the hole spin in the X^- in ZnO, one can extrapolate the $\rho(t)$ curve for the QW to $t = 0$. An initial optical orientation of $\rho(0) = 0.35$ follows despite the elapsed localization accompanied by an energy loss of 5 meV. In the insets of Fig. 3, additionally the magnetic field dependences of hole spin relaxation are given, uncovering a very moderate increase (<8%) of $\tau_1^{s,h}$ for both

X_A^- and D^0X_A with rising $B_\parallel$. Since the p-like hole states usually have a negligible overlap with potentially magnetic nuclei, a contribution from a magnetic field dependent HFI [2] is not expected here. We attribute tentatively the slight increase to the growing energy necessary to flip between the Zeemann split hole states.

In order to study the spin dynamics of resident electrons, we concentrate on D^0X. A technique is applied which has been used to study the electron spin in charged CdSe quantum dots [8]. The PL detection is fixed on σ^+ polarization, while the excitation is periodically alternating between the opposite helicities with a duty cycle of 1:1 and fixed periods T_p. σ^+ polarized photons resonant to the D^0X_B transition can only address spin-up donor electrons along the blue arrow of the left arm in Fig. 2(b). After very fast conversion from the D^0X_B to the D^0X_A state as discussed above, donor bound exciton can recombine via the left arm with σ^- photon emission, or decay, after hole spin flip with σ^+ photon emission. As a result of continuous σ^+ pumping, the spin-up state of the resident electron increasingly depopulates, whereas the spin-down state increasingly populates. Switching now to σ^- excitation via D^0X_B, the absorption starts from a value larger than that for equally populated spin states followed by a successive absorption bleaching due to now active reversed spin pumping. Since the absorption at the D^0X_B transition is clearly smaller than unity [see Fig. 1(b)], the ongoing absorption bleaching can be simply monitored via the PL as long as τ_d remains negligible against the time constant of spin pumping. In principle, a similar scheme can be applied for spin pumping of resident electrons in QWs via the charged exciton, where even the B to A hole conversion is avoided by pumping at the X_A^- absorption peak. However, the combined action of hole spin flip and electron-hole recombination used for electron spin pumping is accompanied here by localization processes. Due to the involved different localization sites, it cannot be safely adopted that the spin polarized electrons are addressed completely by the subsequent excitation at about 5 meV higher photon energies. We note, that qualitative features of resident electron spin pumping have been observed for the QW sample in principal agreement with the data for D^0X which will be analyzed quantitatively in the following.

The PL transients of D^0X are plotted in the upper inset of Fig. 4 for $T_p = 10$ μs at $B_\parallel = 6$ mT in accord with the above predicted behavior. The amplitude A_s defined as the enhancement of the PL intensity just after the excitation polarization switching against the equilibrium value (normalized to unity), is a direct measure of the achieved spin polarization [8]. The $B_\parallel$ dependence of A_s is plotted in Fig. 4. The field dependence uncovers the physical origin behind [2,19]; the HFI is increasingly inhibited by a proper magnetic field applied along the spin quantization axis. As seen, a modulus of $|B_\parallel| = 2.5$ mT is large enough to suppress effectively the spin relaxation of donor electrons by the fluctuating Overhauser field B_N stemming from the magnetic nuclei [20]. Taking the exciton Bohr radius $a_B = 1.4$ nm [10] as an upper measure for the volume seen by the donor electron and the natural abundance of 4% for magnetic Zn nuclei, one ends up with an estimation of slightly larger than 10 for the total amount of magnetic nuclei N_m inside the ZnO donor, explaining the small value of B_N here as seen from the following comparison.

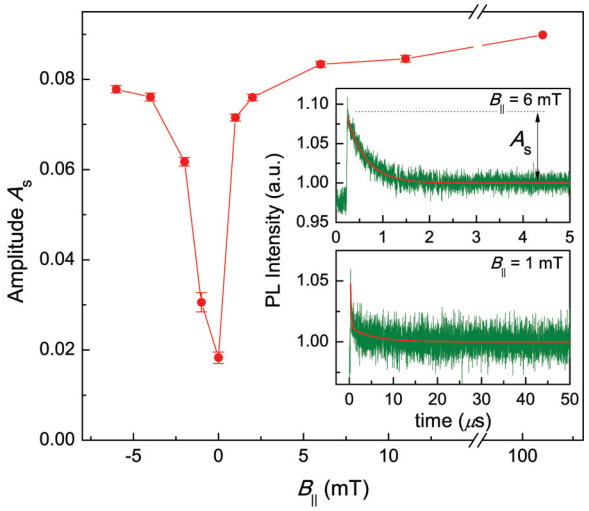

FIG. 4. $B_\parallel$ dependence of spin amplitude A_s taken for a period of $T_p = 10$ μs for alternating helicity of excitation. Upper and lower inset: D^0X_A PL transient after switching from σ^+ to σ^- polarized excitation at $t = 0$ for $T_p = 10$ μs, $B_\parallel = 6$ mT and $T_p = 130$ μs, $B_\parallel = 1$ mT, respectively.

N_m is more than one order of magnitude smaller than in CdSe quantum dots with typical $B_N \approx 100$ mT [8] and three orders of magnitude smaller than N_m in InAs quantum dots with B_N in the several T range [2].

Since the D^0X absorption bleaching is a nonlinear process, the visible time constant τ_{eff} is not directly related to the longitudinal electron spin relaxation time. The underlying rate equation for the population n_+ of spin-up states reads [2,8]

$$\dot{n}_+ = g^* n_- - \frac{n_+ - n_-}{2\tau_1^{s,e}} \tag{1}$$

with an effective pump rate g^* and $n_0 = n_+ + n_-$ as the total number of dressed spin states. The spin relaxation rate seen in the transient in the upper inset of Fig. 4 is then given by $1/\tau_{\text{eff}} = g^* + 1/\tau_1^{s,e}$. In Fig. 5, this rate is plotted versus excitation intensity $I \propto g^*$ for $B_\parallel = 10$ mT with inhibited HFI. From the

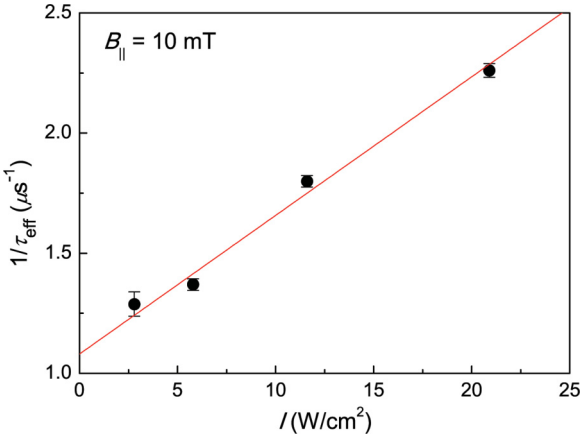

FIG. 5. $1/\tau_{\text{eff}}$ versus excitation intensity I plot to extract the longitudinal electron spin relaxation time in the case of inhibited HFI due to $B_\parallel = 10$ mT.

interception with the ordinate, a value of $\tau_1^{s,e} = 900$ ns follows under these circumstances. This value is in rough accord with a more recently published estimation $\tau_1^{s,e} > 200$ ns obtained from spin-noise spectroscopy for the ZnO donor electron in a varying longitudinal magnetic field $B_\parallel \leqslant B_N$ [21]. Whether the observed value in the 1 μs range represents already the upper limit arising from the D'yakonov-Perel mechanism is presently not known. The longest spin coherence times $\tau_2^{s,e}$ of the donor electron in ZnO reported so far are about 40 times shorter [21,22] pointing to possible improvements for the use in prototype spintronic devices.

For $B_\parallel < 2$ mT, a dynamic nuclear polarization (DNP) is expected due to the HFI between donor electron spin and involved magnetic nuclei, which in turn stabilizes the electron spin [8]. The presence of such a process in ZnO is proven by the characteristic transient in the lower inset of Fig. 4 taken with much longer $T_p = 130$ μs at $B_\parallel = 1$ mT. Besides the fast component already known from the upper inset (note the quite different time scales for both insets), a slow component signifies the progressive establishing of a DNP. Its amplitude is about one order of magnitude smaller than A_s at inhibited HFI indicating also the restricted number of nuclei interacting with the donor electron.

IV. CONCLUSIONS

In summary, we have measured the longitudinal hole spin relaxation time of 80 and 140 ps for D^0X and X^-, respectively. HFI between the resident electron of D^0X and nuclei can be suppressed with very small external magnetic field range of about 2 mT and the longitudinal spin relaxation time of donor electrons reaches values in the 1 μs range. The study has revealed that the spin properties of ZnO differ significantly from those of the *usual* compound zinc-blende semiconductors, which is caused by the comparable small abundance of magnetic nuclei as well as small SO interaction.

ACKNOWLEDGMENT

This work was supported by the Deutsche Forschungsgemeinschaft Grant No. He1939/22-2 within the Priority Program SPP 1285.

[1] C. Klingshirn, Phys. Status Solidi B **244**, 3027 (2007).
[2] *Spin Physics in Semiconductors*, edited M. I. Dyakonov (Springer, Berlin, 2008).
[3] S. Ghosh, V. Sih, W. H. Lau, and D. D. Awschalom, Appl. Phys. Lett. **86**, 232507 (2005).
[4] D. Lagarde, A. Balocchi, P. Renucci, H. Carrère, F. Zhao, T. Amand, X. Marie, Z. X. Mei, X. L. Du, and Q. K. Xue, Phys. Rev. B **78**, 033203 (2008).
[5] D. Lagarde, A. Balocchi, P. Renucci, H. Carrere, T. Amand, X. Marie, Z. X. Mei, and X. L. Du, Phys. Rev. B **79**, 045204 (2009).
[6] W. M. Chen, I. A. Buyanova, A. Murayama, T. Furuta, Y. Oka, D. P. Norton, S. J. Pearton, A. Osinsky, and J. W. Dong, Appl. Phys. Lett. **92**, 092103 (2008).
[7] J. Puls, S. Sadofev, and F. Henneberger, Phys. Rev. B **85**, 041307(R) (2012).
[8] I. A. Akimov, D. H. Feng, and F. Henneberger, Phys. Rev. Lett. **97**, 056602 (2006).
[9] S. Sadofev, S. Blumstengel, J. Cui, J. Puls, S. Rogaschewski, P. Schäfer, Y. G. Sadofyev, and F. Henneberger, Appl. Phys. Lett. **87**, 091903 (2005).
[10] J. J. Hopfield, J. Phys. Chem. Solids **15**, 97 (1960); D. G. Thomas, *ibid.* **15**, 86 (1960).
[11] A. V. Rodina, M. Strassburg, M. Dworzak, U. Haboeck, A. Hoffmann, A. Zeuner, H. R. Alves, D. M. Hofmann, and B. K. Meyer, Phys. Rev. B **69**, 125206 (2004).
[12] J. Puls, F. Henneberger, and J. Voigt, Phys. Status Solidi B **119**, 291 (1983).
[13] M. R. Wagner, G. Callsen, J. S. Reparaz, J.-H. Schulze, R. Kirste, M. Cobet, I. A. Ostapenko, S. Rodt, C. Nenstiel, M. Kaiser, A. Hoffmann, A. V. Rodina, M. R. Phillips, S. Lautenschläger, S. Eisermann, and B. K. Meyer, Phys. Rev. B **84**, 035313 (2011).
[14] Fang-Yi Jen, Yen-Cheng Lu, Cheng-Yen Chen, Hsiang-Chen Wang, C. C. Yang, Bao-ping Zhang, and Y. Segawa, Appl. Phys. Lett. **87**, 252117 (2005).
[15] D. J. Hilton and C. L. Tang, Phys. Rev. Lett. **89**, 146601 (2002).
[16] G. E. Pikus and A. N. Titkov, in *Optical Orientation*, edited F. Meier and B. P. Zakharchenya (North-Holland Physics, Amsterdam, 1984), Chap. 3.
[17] M. Syperek, D. R. Yakovlev, A. Greilich, J. Misiewicz, M. Bayer, D. Reuter, and A. D. Wieck, Phys. Rev. Lett. **99**, 187401 (2007).
[18] E. A. Zhukov, D. R. Yakovlev, M. Gerbracht, G. V. Mikhailov, G. Karczewski, T. Wojtowicz, J. Kossut, and M. Bayer, Phys. Rev. B **79**, 155318 (2009).
[19] V. Gapon, J. Puls, and F. Henneberger, Appl. Phys. Lett. **94**, 213111 (2009).
[20] For the Overhauser field arising from N_m independent nuclear spins, the ratio between the fluctuation σ_{B_N} and the field strength of completely aligned spins is given by $1/\sqrt{N_m} \approx 0.3$. Therefore, the field $B_\parallel$ necessary to suppress the HFI represents a good estimation of B_N in the case of ZnO.
[21] J. Hübner, F. Berski, R. Dahbashi, and M. Oestreich, Phys. Status Solidi B **251**, 1824 (2014); H. Horn, A. Balocchi, X. Marie, A. Bakin, A. Waag, M. Oestreich, and J. Hübner, Phys. Rev. B **87**, 045312 (2013).
[22] S. Kuhlen, R. Ledesch, R. de Winter, M. Althammer, S. T. B. Gönnenwein, M. Opel, R. Gross, T. A. Wassner, M. S. Brandt, and B. Beschoten, Phys. Status Solidi B **251**, 1861 (2014).